Iterative least–squares–based wave measurement using X–band nautical radar

3 authors, including:

Weimin Huang
Memorial University of Newfoundland
290 PUBLICATIONS **4,090** CITATIONS

Eric W. Gill
Memorial University of Newfoundland
194 PUBLICATIONS **3,313** CITATIONS

Iterative Least-squares-based Wave Measurement Using X-band Nautical Radar

Weimin Huang, *Senior Member, IEEE,* Eric Gill, *Senior Member, IEEE,*

Jiaqi An, *Student Member, IEEE*

Abstract

In this paper, an existing iterative least-squares (LS) method for determining ocean surface currents from X-band nautical radar images is modified for extracting ocean wave information from the same data. Within each iterative step, the image spectra samples are classified as containing contributions from fundamental, first-order harmonic, and higher harmonics waves or noise. Based on the classification result, a new scheme is proposed to increase the robustness of current estimation. This involves automatically adjusting the first threshold that is used for obtaining an initial guess of the current velocity in the iterative LS method. The proposed wave algorithm directly uses the classified fundamental and first-order harmonic wave components for wave spectra and parameter retrieval. Unlike previous wave analysis techniques in which a band-pass filter is required to eliminate the non-wave contributions after the current velocity is obtained, the proposed algorithm simplifies the wave retrieval without such a band-pass filter. Harmonic wave components are also accounted for in the wave retrieval process. Algorithm verification is first conducted using simulated radar images. Subsequently, the method is applied to field radar data and the results are compared with wave-buoy measurements. Wave parameters from both types of data show that the modified wave algorithm produces results that are close to those achieved using traditional algorithms. The vertically-polarized radar is also found able to measure wave parameters under low sea states.

Index Terms

Nautical radar, wave measurement.

I. INTRODUCTION

X-band nautical radar has been successfully employed in collecting ocean surface information such as wave parameters [1]-[6], current velocity [7]-[9] and the surface wind field [10] for nearly three decades. It has also been used for investigating sea floor bathymetry [11]-[12] . In 1985, Young *et al.* [1] first extracted directional wave spectra from a series of gray-scaled radar image sequences using a 3-D fast Fourier transform (FFT)-based algorithm. Subsequently, significant effort has been expended in improving and validating the wave algorithm [2]-[6]. However, all existing wave algorithms involve applying a band-pass filter (BPF) after the sea surface current velocity is obtained. The main purpose of such a band-pass filter is to remove the non-wave contribution from the image spectra using the current-included wave dispersion relationship.

Among the various current algorithms available, the normalized scalar product (NSP) method, which was recently presented by Serafino *et al.* [9], is very robust even at high speed current of encounter. The iterative least-squares (LS) method [7] is traditional but widely used. In the iterative LS current method, the samples of the image spectra are classified as contributions from the fundamental, first-order harmonic, and higher harmonics waves or noise. Since the classification procedure already distinguishes between the wave and non-wave components, the results may be used for wave information extraction directly without subsequently band-pass filtering. In this paper, a simplified wave algorithm based on the iterative LS current method is presented. Since it is to be used for comparison purpose, the usual 3-D Fourier-based wave algorithm is briefly introduced in Section II. Then, in Section III, the details of the proposed wave algorithm based on the iterative LS current method and the new threshold-adjusting scheme are described. Results from simulations and field tests are provided and analyzed in Section IV. Conclusions and future work are outlined in Section V.

II. REGULAR WAVE ALGORITHM

Existing algorithms for wave information extraction from nautical radar images consist of the following key steps:

1) obtaining 3-D image spectra by applying a 3-D FFT on a temporal sequence of 32 or 64 sub-images;

2) high-pass filtering the image spectra to eliminate non-stationary and non-homogeneous components;

3) determining current velocity with appropriate methods (e.g., [7]-[9]);

4) band-pass filtering to discriminate the fundamental wave from undesired components using the current-included dispersion relationship;

5) converting the filtered image spectra to wave spectra using a modulation transfer function to minimize the non-linearity due to the radar imaging mechanism;

6) deriving wave spectra and parameters.

As may be observed, in this procedure a band-pass filter is always used after the current velocity is obtained. The 3-D band-pass filter may be designed in the angular frequency and wave vector domain [13], [14] using the fundamental mode wave dispersion relationship in which the current velocity is incorporated. Thus, the components that fall in the pass band of the filter are regarded as contributions from fundamental waves only, and the correspondingly derived spectrum and wave parameters will not include the harmonic wave contribution.

III. SIMPLIFIED WAVE ALGORITHM

Here, a simplified wave algorithm, which does not require further band-pass filtering beyond that necessary for current retrieval, is proposed. Its basic idea lies in the iterative LS current method in which two thresholding procedures are involved [7]. The first threshold is used to obtain an initial guess of current velocity by considering the fundamental mode dispersion relation, and the second threshold is applied to refine the current result by taking into account the fundamental mode, the harmonics and their aliased dispersion shells with more image spectral points. In [7], the two thresholds are set empirically as 0.2 and 0.02 of the maximum of the image spectral value. In that method, an optimal value of the current velocity, $\vec{u}_e$, is found by minimizing

$$\sum_{i,m,n}^{N} \left(\left| \omega_i - \omega_{p,r}(\vec{k}_{mn}) \right|^2 \right) \tag{1}$$

where N is the number of image spectral points $I(\vec{k}_{mn}, \omega_i)$ with normalized energy higher than the second threshold (e.g., 0.02 in [7]); $\vec{k}_{mn}$ is the sample wave vector and ω_i the sample angular

frequency; $\omega_{p,r}(\vec{k}_{mn})$ is the folded frequency obtained from the theoretical frequency $\omega_p(\vec{k}_{mn})$ or $\omega_p(-\vec{k}_{mn})$ through mapping according to the $2\omega_N$ periodicity, ω_N being the Nyquist frequency, and Hermitian property as previously mentioned in [13]; r is an integer used to specify the frequency interval $[r\omega_N, (r+1)\omega_N]$ and is referred to as the frequency interval index. The theoretical frequency is calculated from the Doppler shifted wave dispersion relationship at the pth $(p = 0, 1, \ldots)$ harmonic using an initial value of $\vec{u}_e$. That is,

$$\omega_p(\vec{k}) = (p+1)\sqrt{\frac{gk}{p+1}} + \vec{k} \cdot \vec{u}_e \qquad (2)$$

where g is the acceleration due to gravity ($g = 9.8$ m/s^2), and $\vec{k}$ is the usual ocean wave vector. For the spectral point $I(\vec{k}_{mn}, \omega_i)$, $\omega_{p,r}(\vec{k}_{mn})$ is found using the following rules:

1) If $\omega_p(\vec{k}_{mn}) \in [r\omega_N, (r+1)\omega_N]$ where $r = 0$ or 2, $\omega_{p,r}(\vec{k}_{mn}) = \omega_p(\vec{k}_{mn}) - r\omega_N$

2) If $\omega_p(-\vec{k}_{mn}) \in [r\omega_N, (r+1)\omega_N]$ where $r = -1$ or 1, $\omega_{p,r}(\vec{k}_{mn}) = -\omega_p(-\vec{k}_{mn}) + (r+1)\omega_N$

3) Otherwise, this spectral point will not be included for current calculation.

For the qualified spectral value $I(\vec{k}_{mn}, \omega_i)$, all possible associated folded frequencies $\omega_{p,r}(\vec{k}_{mn})$ fall in $[0, \omega_N]$. Mode classification of $I(\vec{k}_{mn}, \omega_i)$ to determine the only possible combination of mode p and frequency interval index r is performed by comparing the difference between all possible folded frequencies associated with this value and the sample frequency ω_i. If the minimum distance between the folded frequency and sample frequency satisfies

$$\underset{p,\,r}{\text{Min}}\,\left(\left|\omega_i - \omega_{p,r}(\vec{k}_{mn})\right|\right) < \Delta\omega \qquad (3)$$

where $\Delta\omega$ is the frequency resolution of the image spectra, the spectral point $I(\vec{k}_{mn}, \omega_i)$ and its associated p and r will be used to estimate a new current velocity $\vec{u}_e$ by least-squares fitting as outlined in [7]. This new current velocity is then used for updating p and r. The above procedure is repeated until an optimal current velocity is obtained using an iteration termination criterion as given in [15], [16]. However, the initial guess for the current velocity strongly depends on the choice of the first threshold. A wrong threshold value can result in a wrong current result and affect subsequent analysis (as seen in [16], in which some abnormal results with large error were observed). The value may be adjusted according to the signal to noise ratio [7]. Here, a new scheme for choosing the thresholds for current estimation is used. Since the selection of the second threshold is less sensitive, it is fixed as a value between 0.005 and 0.02 because the spectral points with normalized energy lower than this value are trivial for wave retrieval. Only

the first threshold which may be set as 0.2 (as in [7]) initially and is adjusted automatically after the wave components classification with two thresholding procedures. It is found that the wave components classification result varies with the adjusted first threshold, but it becomes more stable when the threshold is close to being optimal. If the number of first-order or higher-order harmonics is larger than that of the fundamental modes, the first threshold is reduced by 0.005. This procedure is repeated until a satisfactory result is obtained. With this scheme, abnormal current velocity points can be reduced.

It is obvious that once the optimal current velocity is found, the wave mode p and frequency interval index r of all the N spectral points whose energy is higher than the second threshold are also known. Here, only the fundamental ($p = 0$) and first-order harmonic ($p = 1$) waves are considered. The frequency interval index r ($r = -1, 0, 1, 2$) enables the back-folding for spectral points with $\omega_i \in [0, \omega_N]$ to $\omega_{ir} \in [-\omega_N, 3\omega_N]$. It should be noted that higher value of r should be used for radar data from fast ships since strong spectral folding may occur. Since, during the iterative process, the samples are already classified as contributions from the fundamental, 1st-order harmonic, higher order wave components or noise, a subsequent band-pass filter to remove higher order harmonic waves and noise is not required. In this paper, the spectral points $I(\vec{k}_{mn}, \omega_i)$ classified as fundamental and first-order harmonic are both used for deriving the wave spectrum $E(\omega, \theta)$ as well as wave parameters. It should be noted also that harmonics in the image spectrum may result from the imaging non-linearity. These harmonics cannot be distinguished from the wave harmonics if both are located on the dispersion shell. In order to reduce the influence of the imaging non-linearity on wave spectra retrieval, a modulation transfer function (MTF) is usually used (see next section for more details).

IV. RESULTS AND ANALYSIS

A. Simulation Result

The proposed wave algorithm is first tested using simulated radar images. By considering both shadowing (SH) and tilt modulation (TM) [17], [18], the simulated radar images used here are generated using the ITTC wave spectrum [19] with the parameters listed in Table I.

Due to the radar imaging mechanism (i.e., SH and TM), the difference between the radar image spectrum and wave spectrum needs to be minimized by using MTF of the form [17]

$$|M(k)|^2 = F_{radar}(k)/F_{true}(k) \propto k^\beta$$

TABLE I

SIMULATION PARAMETERS

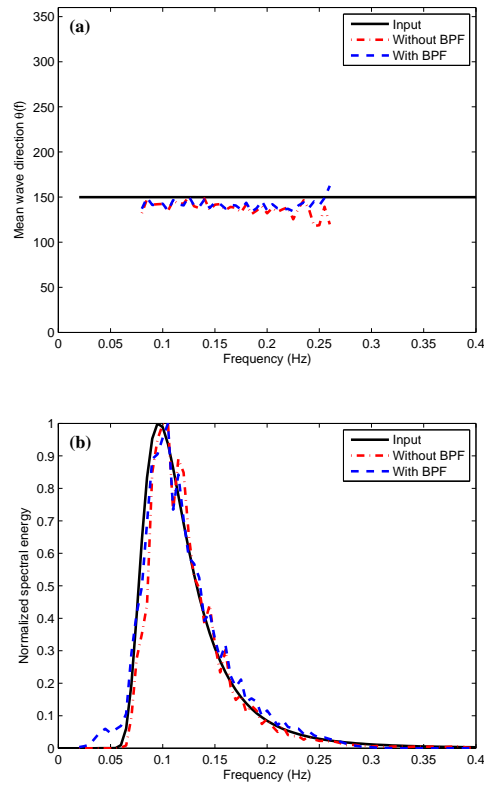|	
Radar frequency	10 GHz
Antenna angular speed	48 r.p.m.
Antenna height	20 m
Range resolution ($\Delta R = \frac{c\tau}{2}$)	10.5 m
Image Size	512×512 pixels
Significant wave height	2.5 m
Directional distribution	Cosine squared
Current velocity	1.00 (m/s)
Current direction	$150°$

Fig. 1. Comparison of results from simulated radar images: (a) Mean wave direction $\theta(f)$; (b) 1-D frequency wave spectrum $E(f)$.

where k is wave number, and $F_{radar}(k))$ and $F_{true}(k)$ are the radar-derived 1-D wavenumber spectrum and true wave spectrum, respectively. It should be noted that the MTF exponent is found using the normalized 1-D wavenumber spectra. This is different from the traditional method [20]-[21] which consists of using a different MTF to scale the spectral energy for each $\vec{K}$ in each frequency plane of the 3D-FFT output. In [17], it was found that the MTF exponent does not differ significantly under varying sea states and it is regarded as an empirical constant. In [17], the transfer function exponent β is estimated as 1.2 based on extensive simulation analysis. Here, this same value is used for our simulated data. Fig. 1 illustrates a comparison of the retrieved results using the traditional (with BPF) [3] and simplified (without BPF) algorithms for identical input spectra. From Fig. 1(a), it is seen that the mean wave direction $\theta(f)$ is recovered correctly in general with both algorithms. Here, the derived mean wave direction is provided only for the frequency range of $[0.08, 0.26]$ Hz since larger errors would appear at very low or high frequencies due to the low energy for these wave components. Over this frequency range, the root mean square errors (RMSEs) of the mean wave direction for the traditional and proposed algorithms are $10°$ and $13°$, respectively. Fig. 1(b) depicts the agreement between the input and extracted non-directional (1-D) frequency wave spectra $E(f)$. Since the proposed method is not aiming to obtain the absolute spectral amplitude, only normalized wave spectra are depicted here. It can be seen that the performances of the simplified and traditional algorithms are almost identical except at the low and high frequency bands. At both low and high frequency ends, $E(f)$ obtained from the simplified algorithm is a little lower than both the input and that from the traditional one. This is to be expected since the wave components or noise with normalized energy lower than the threshold of the current method are eliminated and not accounted for in the new wave retrieval scheme. The same reason may also be used to explain why the simplified algorithm provides better results at the low frequency end. Other input and retrieved wave parameters are listed in Table II from which it can be seen that the retrieved wave parameters agree well with the corresponding input values. It should be noted that the peak wave direction estimation errors are about $10°$. This may be attributed, at least partially, to the fact that a wave direction resolution of $5°$ is used to generate the simulated radar images.

TABLE II

COMPARISON OF INPUT AND RETRIEVED WAVE PARAMETERS FROM SIMULATED DATA

Parameters	Input	Without BPF	With BPF
Peak wave direction $\bar{\theta}(°)$	$150°$	$137°$	$137°$
Mean period T_{01} (s)	8.13	7.99	8.20
Peak period (s)	10.53	9.52	9.52

B. Field Result

1) V-pol Data from a Land-based System: The proposed wave algorithm has also been applied to field data collected by dual polarized land-based radars on Dec. 15 and 20, 2010 at Skerries Bight near the St. John's Harbor on East Coast of Canada (see Fig. 2). In order to validate the results from this algorithm, a TRIAXYS wave buoy with an acoustic Doppler current profiler (ADCP) moored approximately 0.6 nautical miles (1.11 km) offshore was employed. Detailed information about the ADCP may be found in [15]. The wave buoy provides wave information every 25 minutes, and the frequency bands of the derived wave spectra range from 0.64 Hz (1.56 seconds) to 0.03 Hz (33.33 seconds) with a resolution of 0.005 Hz. Thus, it is able to provide 123 frequency bands with the first band centred at 0.03 Hz and the last band centred at 0.64 Hz. Here, only the portion from 0.05 to 0.4 Hz is used in order to compare it with the radar results. The buoy-measured significant wave height during the experiment period is 2.2 m. The specification of the radar appears in Table III.

Before extracting wave information, current velocity must be obtained. The methods of deriving current velocities have been discussed in [16] in which it also pointed out that the vertically-polarized (V-pol) radar provided better current results than the horizontally-polarized (H-pol) radar for the available datasets. At low grazing angles, the spatial textures of H-pol and V-pol X-band marine radars are different and Trizna *et al.* [22] found that the H-pol signal exhibits less spatial homogeneity than the V-pol signal. Therefore, only the V-pol data used in [16] are analyzed here. To retrieve one set of the current and wave information, sequences consisting of 64 consecutive radar image subareas, with dimensions of 128×128 pixels, were selected close to the wave buoy. Since the buoy result is an average value over a period of 25 minutes, it is better for the radar data to be averaged over a comparable period. Here, a 20-minute average is used.

Fig. 3 shows an example of image spectrum after the application of a 3D-FFT. In order to convert the image spectrum to a wave spectrum, a proper MTF exponent β needs to be calibrated for each radar system. This value is determined by curve fitting $log(|M(k)|^2)$ and $log(k)$. Here, the buoy-recorded wave number spectrum is regarded as the true spectrum, and the time averaged radar spectrum is used for curve fitting. Figs. 4(a) and (b) depict the curve fitting result with the radar spectrum derived from both the new and the traditional algorithms. The corresponding MTF exponent β is estimated as 0.58 and 0.72, respectively. It is found that the β used for the simplified algorithm is smaller than that for the traditional one. This may be due to the fact that the spectral points with energy lower than the threshold are not used for wave retrieval in the proposed algorithm. However, a smaller β can amplify the relative spectral energy for the high frequency wave components with respect to the peak. Fig. 5 illustrates the comparison of the wave spectra from the radar and buoy data collected on Dec. 15, at which time the radar-derived current speed and direction are 34 cm/s and $81°$, respectively. Fig. 5(a) depicts the mean wave direction $\theta(f)$, and it may be observed that the two curves agree very well for the range of $f \in [0.05, 0.22]$ Hz, within which the RMSEs for the traditional and proposed algorithms are $14°$ and $15°$, respectively. The use of the MTF values along the straight fitting line rather than the actual sample data in Figure 4 may account for some of the difference between the radar-derived and buoy-recorded wave spectra. It should be noted that large errors in the radar-derived spectra are observed for waves with $f > 0.22$ Hz. This is due to the low energy of these high frequency components. For this reason, only the low frequency portion is shown. Fig. 5(b) illustrates the comparison of the non-directional wave frequency spectra. It is clear that the radar-derived frequency spectra agree well with the buoy result even under such a low sea state. The radar-derived spectra obtained from the simplified wave algorithm agree better with the buoy results than those obtained from the traditional method in the low frequency band. However, the same spectra are lower than those derived from the buoy record and the traditional method in the region where the frequency f exceeds 0.20 Hz. The reason for this discrepancy may also be that the samples with spectral energy lower than the second threshold are discarded. The directional wave spectra obtained from radar data are a little less spread than the buoy results (see Fig. 6). This may be due to the model used to derive the directional spectrum from the buoy data. However, from Fig. 6, it is seen that the wave peaks and dominant wave directions from both instruments agree very well with each other. The numerical comparisons of the radar-derived
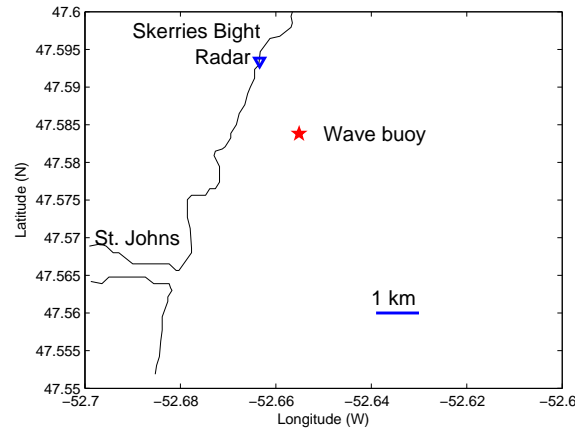
Fig. 2. Radar and buoy site (see also [15]).

TABLE III

RADAR SYSTEM SPECIFICATION

Location	47.59° N 52.66° W
Polarization	Vertical
Antenna angular speed	48 r.p.m.
Radar range resolution (ΔR)	7.51 m
Image Size	1024×1024 pixels

and buoy-recorded wave parameters are listed in Table IV. From Table IV, it may be concluded that the peak wave periods are derived with RMSEs less than 1 s using both wave algorithms, and the differences between the radar and buoy peak wave directions are less than $10°$. It has been considered acceptable if these discrepancies of wave period and wave direction are less than 1.5 s and $25°$, respectively [2], [6].

The results from Dec. 20 are provided in Figures 7-8. On that day, the sea state was much higher (the wind speed was 7.3 knots and the significant wave height was 4.38 m, indicating the likelihood of a swell-dominated sea). All other settings were the same as those on December 15. With the proposed threshold-adjusting scheme, the current velocity abnormalities found in [16] are reduced (see Fig. 9), and the radar-deduced average current speed and direction being 52 cm/s and $95°$, respectively, are comparable to 47 cm/s and $98°$ obtained from the buoy record. Figure 7 depicts the comparison of directional wave spectra derived by the radar and buoy,
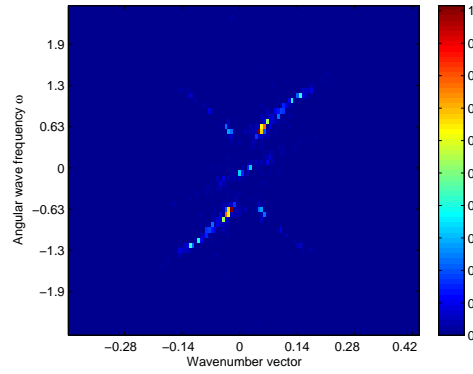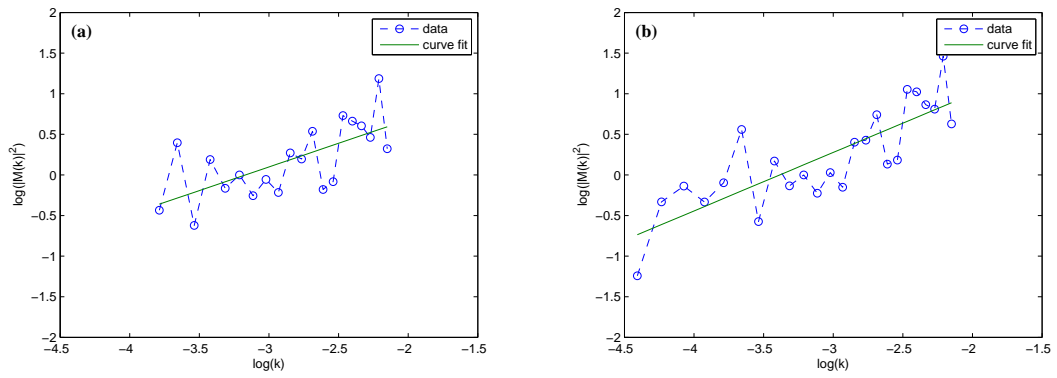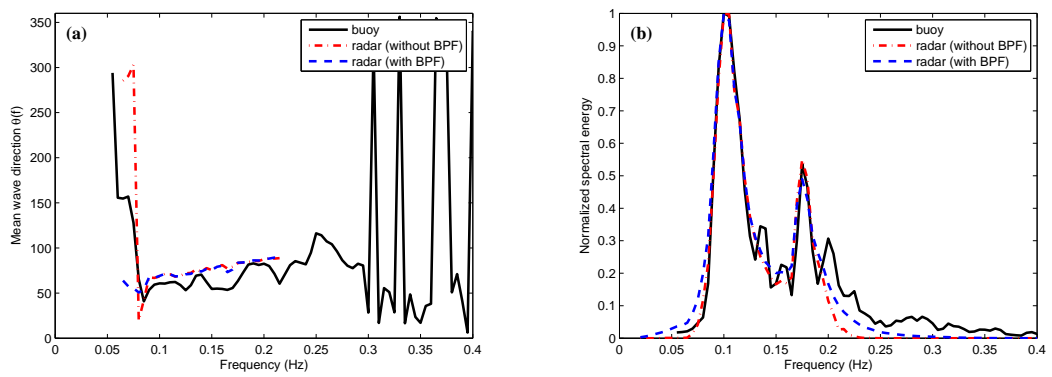
Fig. 3.   Example of an image spectrum $I(\vec{k}, \omega)$.

Fig. 4.   MTF and wave number curve fitting results: (a) without BPF; (b) with BPF.

Fig. 5.   Comparison of results from buoy and radar data collected on Dec. 15: (a) Mean wave direction $\theta(f)$; (b) 1-D wave frequency spectrum $E(f)$.
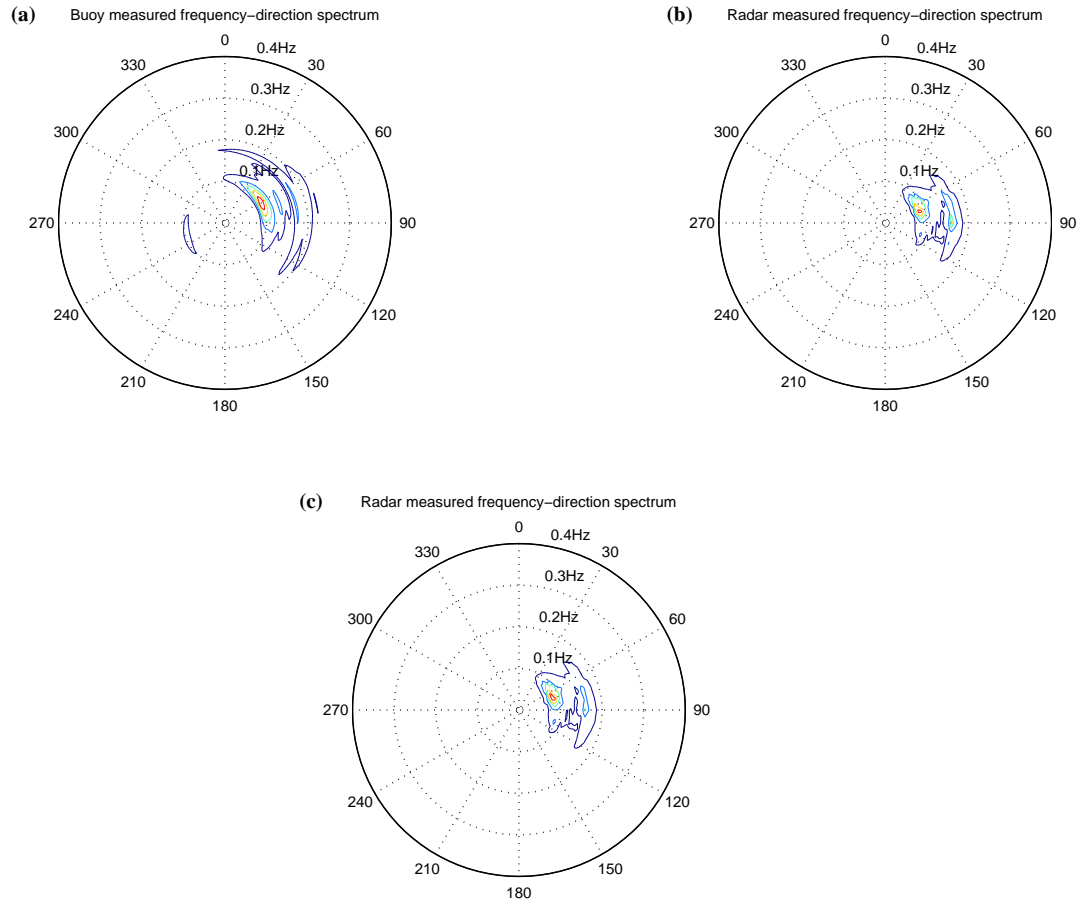
Fig. 6.   Comparison of directional wave spectra $E(f, \theta)$ of Dec. 15: (a) Buoy-recorded; (b) Radar-derived with the simplified algorithm; (c) Radar-derived with the traditional algorithm. The spectrum has been normalized and the contours are drawn from 0.9 to 0.1 in decrements of 0.2.

it also shows that all the spectra are narrower than those obtained from Dec. 15. Figure 8(a) shows good agreement between the mean wave direction obtained from the buoy and radar data over the frequency range of the latter. The RMSEs of the mean wave direction obtained using the traditional and proposed algorithms are $29°$ and $30°$, respectively. The non-directional wave spectra are compared in Fig. 8(b). Two split peaks are visible in the buoy result. The peak of the spectrum extracted by the traditional wave algorithm aligns very well with the first peak, and split peaks are also recovered by the simplified algorithm but the first peak is identified at a little higher frequency. This explains why the peak wave period obtained using the new scheme
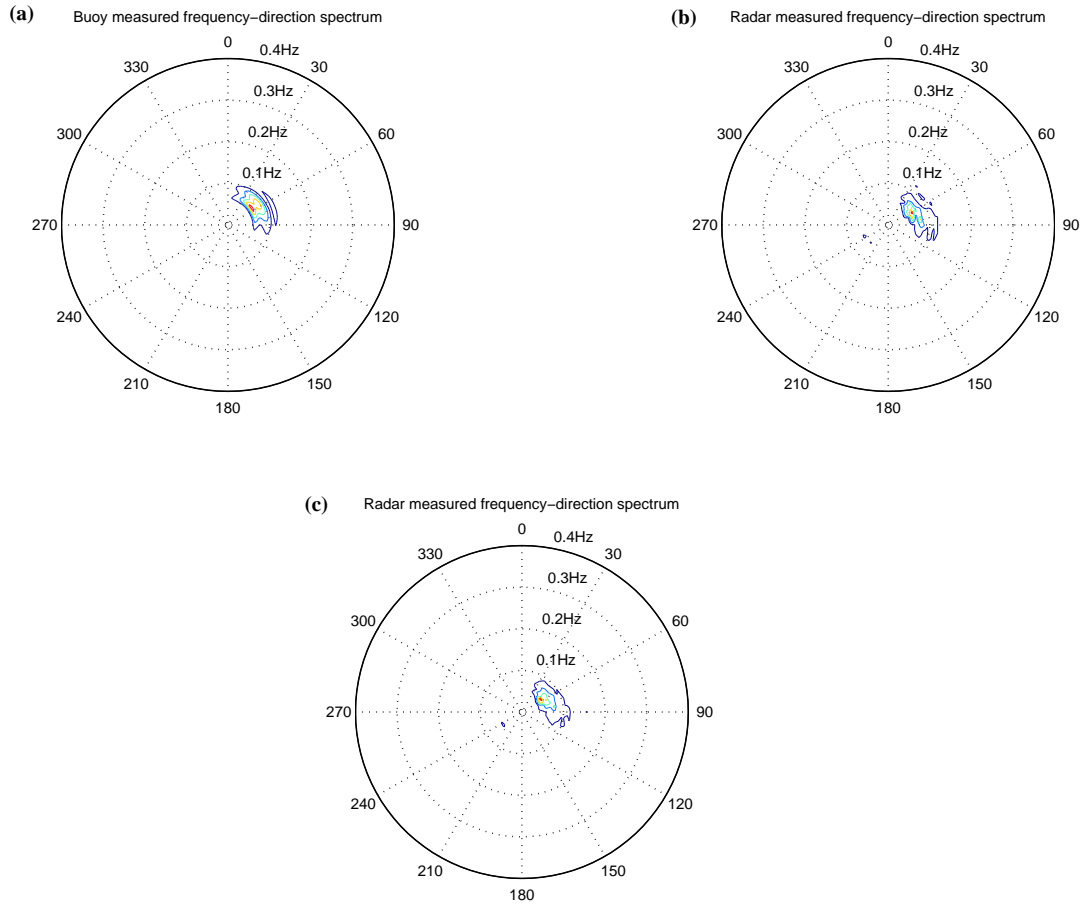
Fig. 7.   Comparison of directional wave spectra $E(f, \theta)$ of Dec. 20: (a) Buoy-recorded; (b) Radar-derived with the simplified algorithm; (c) Radar-derived with the traditional algorithm.

is a little lower than the actual value provided by the buoy as indicated in Table IV.

2) H-pol Data from a Shipborne System: Another larger dataset that was collected with an H-pol shipborne WaMos radar by Defence Research and Development Canada (DRDC) from 14:16 on November 28 to 12:06 on November 29 was analyzed. The antenna rotation speed is 28 r.p.m.. The ship maneuvered within the deep sea area ($42°21.3'$N, $61°55.6'$W) about 220 km Southeast of Halifax. A nearby TRIAXYS buoy at $42°21'$N, $61°53'$W provided wave data every half an hour. The wind speed and wave height time series depicted in Figure 10 are indicators of the sea state during the data collection period. It is also necessary to evaluate the performance of the algorithm under other sea states. Figure 11 shows a comparison of the

TABLE IV

COMPARISON OF DERIVED WAVE PARAMETERS FROM RADAR DATA AND BUOY RECORDS

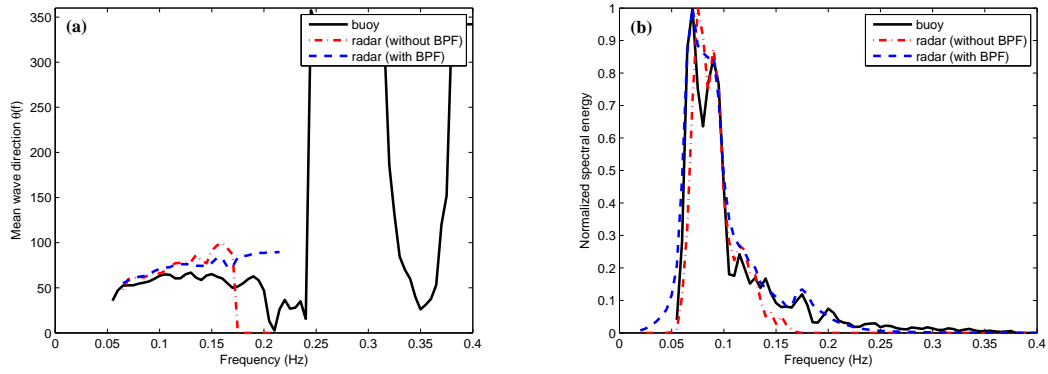| Parameters	Dec. 15			Dec. 20		
	Buoy	Without BPF	With BPF	Buoy	Without BPF	With BPF
Peak wave direction $\bar{\theta}_p(^\circ)$ (w.r.t true North)	61°	68°	69°	53°	61°	58°
Peak wave period T_p(s)	9.52	9.52	9.52	13.33	12.50	13.33

Fig. 8. Comparison of results from buoy and radar data collected Dec. 20: (a) Mean wave direction $\theta(f)$; (b) 1-D wave frequency spectrum $E(f)$.
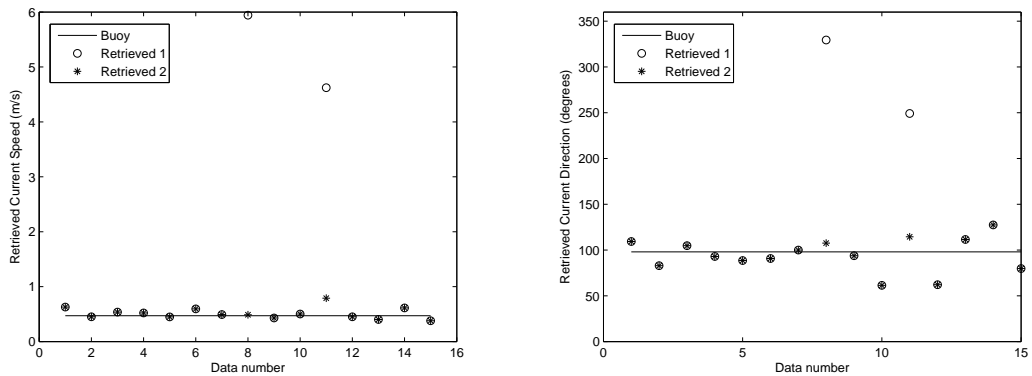

Fig. 9. Comparison of results from buoy and radar data collected on Dec. 20: (a) current speed; (b) current direction. The radar results obtained using the iterative LS method with constant and adjusted first threshold are denoted as "Retrieved 1" and "Retrieved 2", respectively.
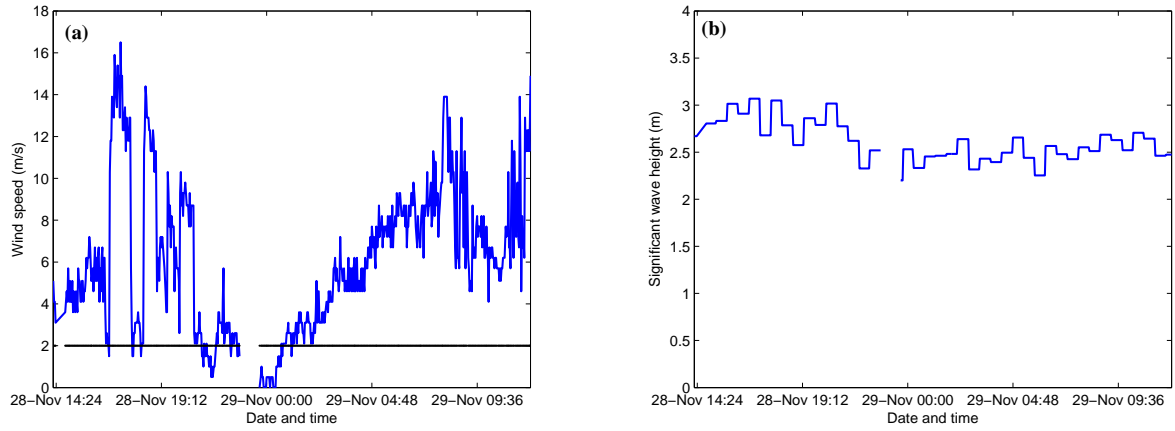
Fig. 10.   Wind speed (a) and wave height (b) variation over time during Nov. 28 - 29. 2008.

radar-derived and buoy-recorded wave spectra under a rough sea state (wind speed of 14.44 m/s and significant wave height of 3.00 m). It may be observed that the radar-derived results using both the simplified algorithm and the traditional method agree well with the buoy measurements. More results are shown in Figure 12. Figures 12 (a) and (b) depict the variation of extracted current speed and direction of encounter (vector sum of current and ship velocities), respectively. The ship velocity is also displayed. It is seen that the extracted results correctly show the ship velocity variation. The peak wave direction and period results derived from the radar data with both the traditional and simplified algorithms are compared with the buoy-recorded result in Figures 12 (c) and (d), respectively. From these two figures, it is seen that results from both algorithms agree well with the buoy result during most of the period. However, the results deviate from the buoy-recorded result for the time around midnight. From Figure 10, it may be observed that the wind speed is lower than 3 m/s from 23:40 on Nov. 28 to 00:40 on Nov. 29. In [23], it is suggested that for H-pol operation a minimum sea surface wind speed of 3 m/s is required to generate a usable level of backscatter for wave measurement. Not including the data falling in this low wind speed period, the RMSEs for the peak wave period are 0.87 s and 0.98 s for the traditional and simplified algorithms; the corresponding errors for peak wave direction are found to be $6.4°$ and $7.3°$, respectively. It should be noted that there are also a few points with larger error in the current speed of encounter (see Figure 12 (a)). This may be due to either (1) the compromising, during low clutter conditions, of the threshold used in the LS current algorithm
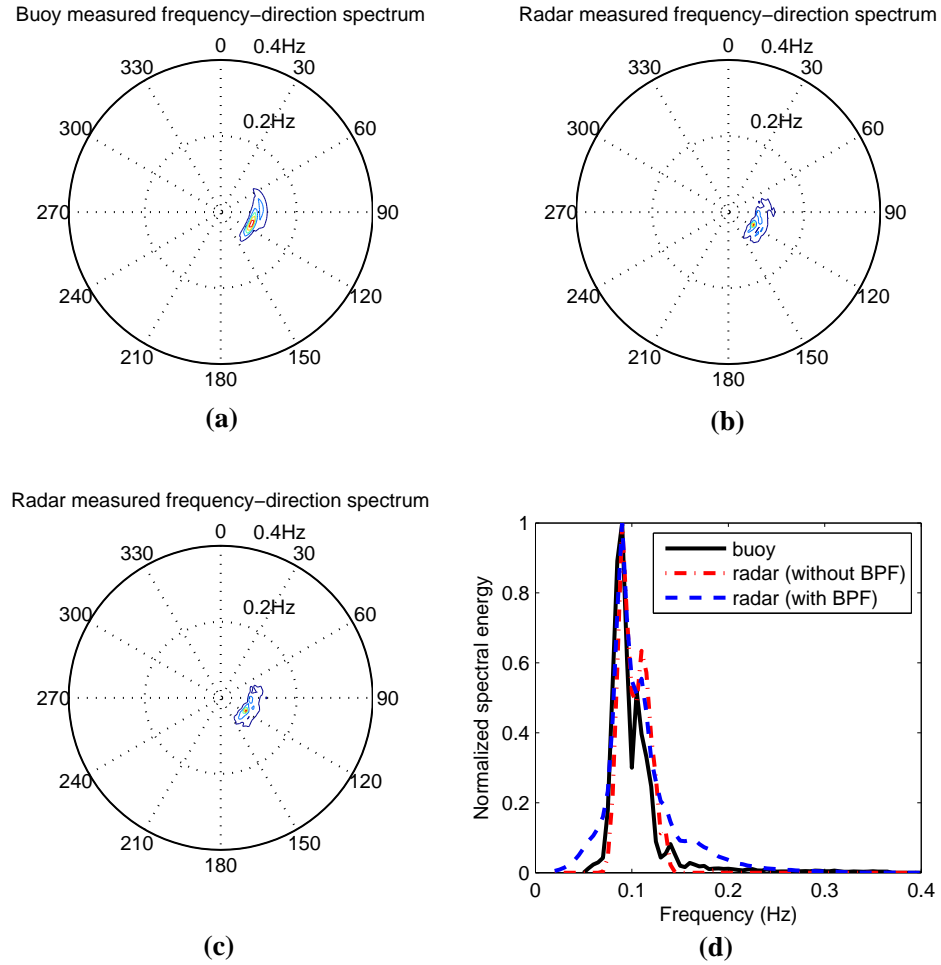
Fig. 11.   Results from buoy and radar data collected under high sea state (wind speed of 14.44 m/s and wave height of 4.80 m) by DRDC at 17:06 on November 28, 2008: (a) Buoy-recorded $E(f, \theta)$; (b) Radar-derived $E(f, \theta)$ with the simplified algorithm; (c) Radar-derived $E(f, \theta)$ with the traditional algorithm; (d) 1-D wave frequency spectrum $E(f)$.

whose performance strongly depends on the choice of that threshold or (2) aliasing arising from large ship speeds. Both of these will result in an imprecise current estimation and significantly affect the subsequent result from the wave algorithm.

V. CONCLUSIONS AND FUTURE WORK

A simplified wave algorithm that uses the contributions of both fundamental and first-order harmonic wave components for wave information retrieval from nautical radar images has been
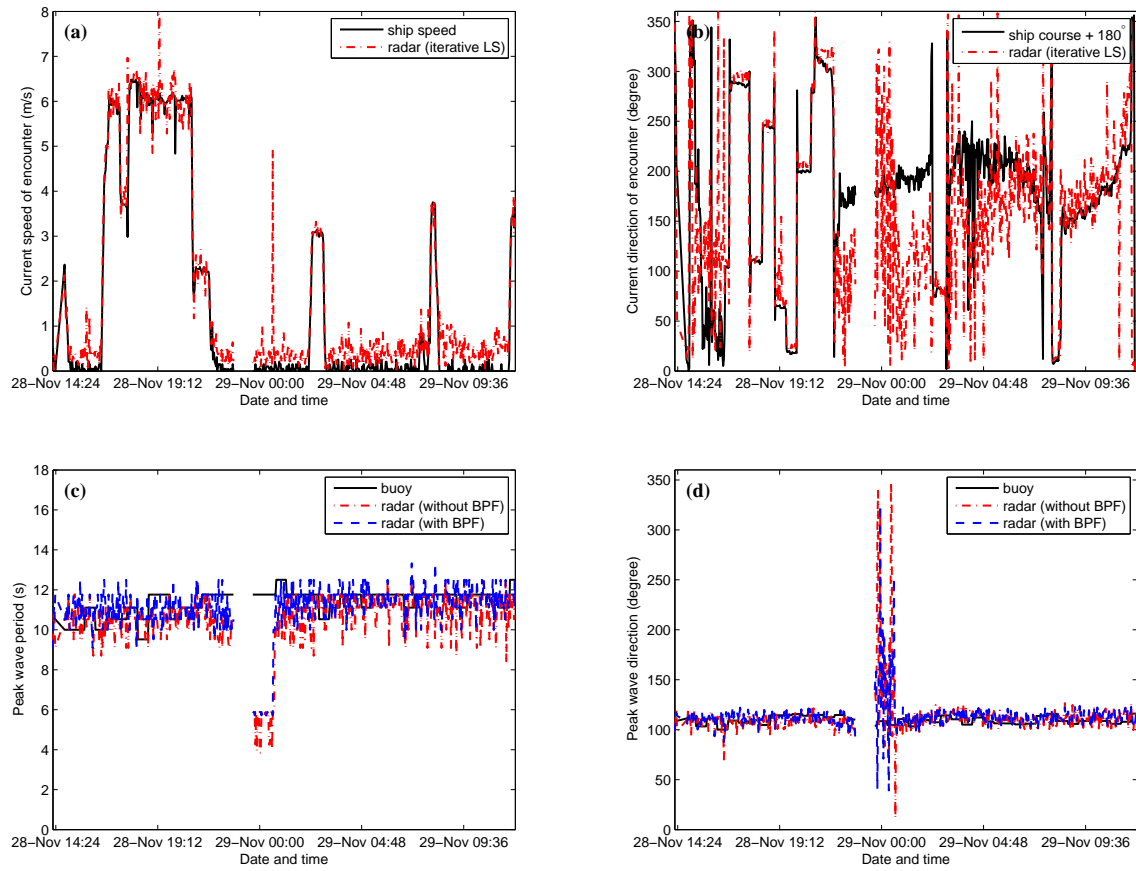
Fig. 12.   Results from buoy and radar data collected by DRDC in November, 2008: (a) Current speed of encounter; (b) Current direction of encounter; (c) Peak wave period; (d) Peak wave direction.

proposed. The algorithm is based on the wave mode classification results obtained using the iterative LS current method. Unlike usual wave algorithms, no band-pass filter is implemented subsequent to the determination of the current velocity. The execution time of the algorithms with and without a BPF is essentially the same. Both can provide real-time wave information retrieval, but, as noted, eliminating the BPF allows for examination of a larger range of wave components. An automatic threshold adjusting scheme is also used to improve the current estimation. The algorithm has been applied to both simulated and field data, and its performance is very close to that of traditional approaches. However, at the high frequency end, wave spectra energy obtained from the simplified algorithm is lower than both the input or the ground-truth as well as that obtained from the traditional approach. This is due to the fact that the wave components

or noise with normalized energy lower than the second threshold of the current method are eliminated and, thus, not accounted for in the new wave retrieval scheme. Although these lower energy components may not affect the retrieval result significantly, a lower second threshold may reduce the spectral difference at high frequencies. The agreement between the radar and buoy results indicates that reliable wave information may be recovered using this simplified algorithm. It is also found that a V-pol system is able to provide wave information under low sea-states. For the data used here, since the highest ship speed is less than 7 m/s, the retrieval results from both the modified and traditional methods are fairly good. The performance using the LS approach may drop with the presence of spectral aliasing when the ship moves with a very high speed. Then, other reference data or other current methods (e.g., NSP [9]) may be used to determine the high current velocity of encounter. Future plans also include the application of the LS-based algorithms to data collected from systems on a vessel moving with very high speed.

ACKNOWLEDGMENT

REFERENCES

[1] Young, I.R., Rosenthal, W., Ziemer, F.: 'A three-dimensional analysis of marine radar images for the determination of ocean wave directionality and surface currents', *J. Geophys. Res.*, 1985, **90**, (C1), pp. 1049–1059.

[2] Izquierdo, P., Guedes Soares, C., Nieto Borge, J.C., Rodriguez, G.R.: 'A comparison of sea-state parameters from nautical radar images and buoy data', *Ocean Eng.*, 2004, **31**, (17-18), pp. 2209–2225.

[3] Nieto Borge, J.C., Guedes Soares, C.: 'Analysis of directional wave fields using X-band navigation radar', *Coastal Eng.*, 2000, **40**, (4), pp. 375–391.

[4] Nieto Borge, J.C., Reichert, K., Dittmer, J.: 'Use of nautical radar as a wave monitoring instrument', *Coastal Eng.*, 1999, **37**, (3-4), pp. 331–342.

[5] Nieto Borge, J.C., Hessner, K., Jarabo-Amores, P., de la Mata-Moya., D.: 'Signal-to-noise ratio analysis to estimate ocean wave heights from X-band marine radar image time series', *IET Radar Sonar Navig.*, 2008, **2**, (1), pp. 35–41.

[6] Cui, L., He, Y., Shen, H., Lu, H.: 'Measurements of ocean wave and current field using dual polarized X-band radar', *Chinese J. Oceanol. Limnol.*, 2010, **28**, (5), pp. 1021–1028.

[7] Senet, C.M., Seemann, J., Ziemer, F.: 'The near-surface current velocity determined from image sequences of the sea surface', *IEEE Trans. Geosci. Remote Sens.*, 2001, **39**, (3), pp. 492–505.

[8] Gangeskar, R.: 'Ocean current estimated from X-band radar sea surface images', *IEEE Trans. Geosci. Remote Sens.*, 2002, **40**, (4), pp. 783–792.

[9] Serafino, F., Lugni, C., Soldovieri, F., 'A novel strategy for the surface current determination from marine X-Band radar data', *IEEE Geosci. Remote Sens. Lett.*, 2010, **7**, (2), pp. 231–235.

[10] Dankert, H., Horstmann, D.: 'A marine radar wind sensor', *J. Atmos. Ocean. Technol.*, 2007, **24**, (9), pp. 1629–1642.

[11] Trizna, D.B.: 'Errors in bathymetric retrievals using linear dispersion in 3-D FFT analysis of marine radar ocean wave imagery', *IEEE Trans. Geosci. Remote Sens.*, 2001, **39**, (11), pp. 2465–2469.

[12] Serafino, F., Lugni, C., Nieto Borge, J.C., Zamparelli, V., Soldovieri, F.: 'Bathymetry determination via X-band radar data: a new strategy and numerical results', *Sensors*, 2010, **10**, (7), pp. 6522–6534.

[13] Nieto Borge, J.C., Ziemer, F., Seemann, J., Senet, C.: 'Overcome the Nyquist limit in frequency in nautical radar measurement of wave fields', Proc. 17th Int. Conf. OMAE, Lisbon, Portugal, July 1998, pp. 1–8.

[14] Reichert, K., Hessner1, K. Nieto Borge, J.C., Dittmer, J.: 'WaMoS II: A Radar based wave and current monitoring system', Proc. Conf. ISOPE '99, Brest, France, May 1999, **3**, pp. 1–5.

[15] Huang, W., Gill, E.: 'Simulation analysis of sea surface current extraction from microwave nautical radar images', Proc. IEEE Int. Conf. Image Process., Orlando, USA, September 2012, pp. 2673–2676.

[16] Huang, W., Gill, E.: 'Surface current measurement under low sea state using dual polarized X-band nautical radar', *IEEE J. Sel. Topics Appl. Earth Observ. Remote Sens. (JSTARS)*, 2012, **5**, (6), pp. 1868–1873.

[17] Nieto Borge, J.C., Rodriguez, R.G., Hessner, K., Gonzales, I.P.: 'Inversion of marine radar images for surface wave analysis', *J. Atmos. Ocean. Technol.*, 2004, **21**, (8), pp. 1291–1300.

[18] An, J., Huang, W., Gill, E.: 'Numerical simulation of X-band marine radar imaging', Proc. IEEE NECEC Conf., Newfoundland, Canada, November 2011, pp. 1–4.

[19] Nomiyama, D.H., Hirayama, T.: 'Evaluation of marine radar as an ocean-wave-field detector through full numerical simulation', *J. Marine Sci. Technol.*, 2003, **8**, (2), pp. 88-98.

[20] Ziemer, F., Rosenthal, W.: 'On the transfer function of a shipborne radar for imaging ocean waves', Proc. IEEE IGARSS Conf., Ann Arbor, USA, July 1987, pp. 1559-1564.

[21] Trizna, D.B.: 'Monitoring coastal processes and ocean wave directional spectra using a marine radar', Proc. MTS/IEEE Oceans, Boston, USA, September 2006, pp. 747–757.

[22] Trizna, D.B., Carlson, D.J.: 'Studies of dual polarized low grazing angle radar sea scatter in nearshore regions', *IEEE Trans. Geosci. Remote Sens.*, 1996, **34**, (3), pp. 747–757.

[23] Nieto Borge, J.C., Guedes Soares, C.: 'Analysis of directional wave fields using X-band navigation radar', *Coastal Eng.*, 2000, **40**, (4), pp. 375–391.